Title

Scanning Laser Ophthalmoscopy Demonstrates Disc and Peripapillary Strain During Horizontal Eye Rotation in Adults.

Authors

Park, Joseph
Moon, Sunghyuk
Lim, Seongjin
et al.

Publication Date

2023-10-01

DOI

10.1016/j.ajo.2023.06.008

Peer reviewed

HHS Public Access

Author manuscript

Am J Ophthalmol. Author manuscript; available in PMC 2024 October 01.

Published in final edited form as:

Am J Ophthalmol. 2023 October ; 254: 114–127. doi:10.1016/j.ajo.2023.06.008.

Scanning Laser Ophthalmoscopy Demonstrates Disc and Peripapillary Strain During Horizontal Eye Rotation in Adults

Joseph Park, Ph.D.[1], **Sunghyuk Moon, M.D.**[1,2], **Seongjin Lim, M.S.**[1,3], **Joseph L. Demer, M.D., Ph.D.**[1,4,5,6]

[1]Department of Ophthalmology, Stein Eye Institute;

[2]Department of Ophthalmology, Busan Paik Hospital, Inje University, Busan, Republic of Korea;

[3]Department of Mechanical Engineering, University of California, Los Angeles;

[4]Neuroscience Interdepartmental Program, University of California, Los Angeles;

[5]Department of Neurology, University of California, Los Angeles;

[6]Department of Bioengineering, University of California, Los Angeles.

Abstract

Purpose: We employed automated image analysis of scanning laser ophthalmoscopy (SLO) to investigate mechanical strains imposed on disc, and retinal and choroidal vessels during horizontal duction in adults.

Design: Deep learning analysis of optical images.

Methods: The peripapillary region was imaged by SLO in central gaze, and 35° ab- and adduction, in younger and older healthy adults. Automated image registration was followed by deep learning-based optical flow analysis to track determine local tissue deformations quantified as horizontal, vertical, and shear strain maps relative to central gaze. Choroidal vessel displacements were observed when fundus pigment was light.

Results—Strains in the retina and disc could be quantified in 22 younger (26±5 years, ±SEM) and 19 older (64±10 years) healthy volunteers. Strains were predominantly horizontal and greater for adduction than abduction. During adduction, maximum horizontal strain was tensile in the nasal hemi-disc, and declined progressively with distance from it. Strain in the temporal hemi-retina during adduction was minimal, except for compressive strain on the disc of older subjects. In abduction, horizontal strains were less and largely confined to the disc, greater in older subjects, and generally tensile. Vertical and shear strains were small. Nasal to the disc, choroidal vessels shifted nasally relative to overlying peripapillary retinal vessels.

Conclusions: Strain analysis during horizontal duction suggests that the optic nerve displaces the optic canal, choroid, and peripapillary sclera relative to the overlying disc and retina. This

Address for Correspondence and Reprints: Joseph L. Demer, M.D., Ph.D., Stein Eye Institute, 100 Stein Plaza, UCLA, Los Angeles, CA 90095-7002. (310) 206-7826 fax; jld@jsei.ucla.edu.

[c]*Authorship*: All authors attest that they meet the current ICMJE criteria for authorship.

Conflict of Interest

No conflicting relationship exists for any author

peripapillary shearing of the optic nerve relative to the choroid and sclera may be a driver of disc tilting and peripapillary atrophy.

Precis for:

Scanning laser ophthalmoscopy was used to image the disc and peripapillary region in central gaze and horizontal ductions. Local strains mapped from image pairs using automated image analysis were greater in adduction than abduction, originated at the disc, and diminished more rapidly in the periphery in older than younger subjects. Retina nasal to the disc bucked in adduction and sheared over the choroid. These eye-movement induced shears might drive maturational disc tilt and peripapillary atrophy.

Keywords

optic nerve tethering; adduction; optical coherence tomography; optic disc

Introduction

The eye is not only a uniquely mobile sensory organ, but forming a central nervous system white matter tract, its optic nerve (ON) passes through a canal and lamina cribrosa in the moving sclera to join the sensory neuroepithelium of the retina. Given that eye movements occur relentlessly during wakefulness and even during sleep[1–5], the mechanical properties of the highly dynamic junction of the ON with the eye have implications for normal visual function, and for common ocular diseases.

The idea that eye movements may transiently deform the optic disc and peripapillary retina is nearly two centuries old. Mechanical stimulation of the peripapillary retina was inferred from gaze-evoked entoptic flashes perceptible near the disc as described by Purkinje in 1836 and Helmholtz in 1911[6]. Friedman reasoned that extreme horizontal ductions must cause ON traction that would deform peripapillary tissues[7]. Such peripapillary deformation accords with modern biomechanical testing of post-mortem human tissues revealing that the peripapillary sclera is one-third to one-fourth as stiff as the contiguous ON sheath[8]. With development of optical coherence tomography (OCT), it became possible to directly image these eye-movement-related disc and peripapillary deformations. Sibony used OCT to demonstrate see-saw deformation of peripapillary Bruch's membrane evoked by horizontal gaze changes in patients with papilledema[9]. This striking phenomenon has been confirmed by raster OCT in normal[10] and esotropic subjects[11], and by 3-dimensional OCT in myopes, yet its cause remains largely unexplained. Raster OCT during horizontal ductions has also demonstrated strain in disc and peripapillary tissues associated with disc drusen[12], as well as lamina cribrosa strain in normal subjects[13]. Confocal reflectance imaging by scanning laser ophthalmoscopy (SLO) has demonstrated that temporal displacements of the bifurcations of disc and peripapillary vessels associated with adduction occur mostly in the nasal half of the disc and are smaller in older than younger healthy subjects[14]. Using a 3-dimensional analysis of OCT, Wang *et al.* have reported nasal compression of the disc in adduction[13].

Beyond occasional phosphenes only perceptible in darkness, the functional significance of disc and peripapillary deformations associated with eye movements has been uncertain.

Sibony and collaborators have proposed that in the setting of calcified optic disc drusen, repetitive tissue shearing due to eye movements may contribute to progressive ON axonal loss[12]. A particular pathological role for adduction in the pathogenesis of normal tension glaucoma (NTG)[13] has been proposed based on the demonstration by magnetic resonance imaging (MRI) that the ON becomes tethered in large angle adduction[15], causing globe retraction by the inelastic ON[16] typical of NTG but not healthy subjects[17]. Traction by the ON in adduction has been suggested as a driver of progressive temporal tilting or torsion of the optic disc, as well as development of peripapillary atrophy[13] and peripapillary staphylomata in axial myopia[18].

Biomechanical simulations using an engineering technique known as finite element analysis (FEA) have been performed to estimate the biomechanical effects of eye movements on the disc and peripapillary tissues. These biomechanical effects are conveniently represented as strain, which can be considered as proportionate deformation in local tissue regions; when excessive or excessively repeated, strain may damage or induce remodeling in tissues. Wang *et al.* performed FEA of a simplified orbit using tissue material parameters from various species, predicting that optic disc strain caused by 13° horizontal eye movements would exceed strain induced by intraocular pressure (IOP) elevation to 50 mmHg[19]. Shin *et al.* implemented FEA of the human disc, sclera, ON, and ON sheath using bovine tissue material parameters, predicting that adduction with ON tethering concentrates stress and strain in the temporal side of the optic disc and peripapillary region, which respond by shifting nasally[20]. Further FEA studies of the effect of material property variations within physiological range of human tissues[21] suggest that such variations around optic disc may concentrate stress and strain on the retrolaminar ON and peripapillary regions during adduction[8,22]. These simulations predict that the temporal disc would shift nasally during adduction tethering of the ON, but paradoxically, imaging by SLO shows that the disc vessel bifurcations[14] and the lamina[13] actually shift temporally relative to the field of view!

The current study aimed to resolve the forgoing paradox through the use of automated analysis of SLO imaging with deep learning-based optical flow to compute the local strains in the optic disc and peripapillary retina based on positions of abundant feature points defined by vessels but are not limited to their relatively sparse bifurcations. From these imaging findings, we present a novel anatomical explanation of relative motion of critical ocular layers that occur during eye rotation.

Methods

Subjects.

This study was conducted prospectively under a protocol approved by the Institutional Review Board of the University of California, Los Angeles, and conforming to tenets of the Declaration of Helsinki. Healthy adult volunteers recruited by advertising gave written informed consent before participation. Subjects underwent ophthalmic examination by an author to verify bilaterally normal corrected visual acuity, normal IOP, and normal ocular anatomy except that pseudophakia was permitted. Subjects were excluded if they had abnormal examination findings, or a history of other ocular surgery, strabismus, or chronic

ocular disease. Repeatability testing was conducted in 10 subjects tested twice at 30-minute intervals.

Data Acquisition.

The Heidelberg Spectralis imager (Heidelberg Engineering, Heidelberg, Germany) was employed in confocal SLO mode that images in infrared; the optical coherence tomography mode was not employed. As depicted in Fig. 1A, the imager rotated about a vertical axis to alter its azimuth angle to follow the same region of the posterior segment in multiple gaze directions. The subject's head position was stabilized with a wide strap and wedge-shaped cushion attached to the scanner headrest. In addition to central gaze, imaging was repeated in 35° ad- and abduction, taking into consideration the offset of the internal fixation target of the scanner as described in a previous study[10]. The scanner exported raw SLO images of 768 × 768 pixels covering an area of approximately 8.9 × 8.9 mm^2 to give a resolution of about 11.6 μm. It should be emphasized that these images were directly acquired in SLO mode and are not *en face* reconstructions of B-scan OCT images.

Image Processing.

Raw images were processed using largely-automated, customized algorithms as illustrated in Fig. 2. Initially, uneven illumination in the raw image was compensated by automatically subtracting local background level. Then, ab- and adducted images were rotated torsionally to match the disc-foveal angle to the central gaze image. After torsional correction, images in ab- and adduction were automatically registered to the central gaze image using the MATLAB implementation of the "speeded-up robust features" (SURF)[23] algorithm, which eliminates large rigid body motion by minimizing differences of the ab- and adducted images from central gaze. This combined approach aligned the images in eccentric gaze positions by compensation for translation and torsion, so that any remaining differences represented deformation associated with the change in eye position.

Local Displacement Estimation Using Optical Flow.

Remaining differences between registered images represent local feature displacements induced by eye rotation. A deep learning-based optical flow algorithm called "recurrent all-pairs field transform" (RAFT)[24] was used to measure local displacement of the non-textured retinal vessels using a context network. Registered image pairs for central gaze versus ab- or adduction were processed using RAFT to generate displacement fields based on correlated features and contexts in the images. A pretrained model provided by Teed *et al.*[24] was used to determine local retinal vascular displacement.

Retinal Vascular Mask Generation.

After estimating the displacement field of the optic disc using RAFT optical flow, retinal background was removed using a mask, leaving only the retinal vessels that were selected for quantitative analysis. This excluded imaging noise otherwise resulting from spurious correlations in the non-vascular retinal background, as well as correlated but oppositely directed relative motion between retinal and underlying choroidal vessels. A retinal vascular mask was generated using a convolutional neural network (CNN) to measure only retinal

vascular displacements. For efficient training, a modified Attention Deeplabv3+, which replaced the backbone of the feature extractor with ResNet-101 and simplified the decoder, was chosen as the CNN[25,26]. A set of 99 images of 768 × 768 pixels were used to train the neural network, with flips, rotations, and elastic distortions augmenting the training dataset. Weighted cross-entropy was chosen as training metric to compensate for the imbalanced number of pixels per anatomic class. Weights were 0.01, 0.05, and 0.25, respectively, for background, blood vessels, and optic disc. The optimizer was Adam, with its learning rate set to 0.0001.

Strain Conversion From Displacement.

After we determined the retinal vascular displacement field, we converted it into a Green-Lagrange strain tensor map as shown in Fig. 3. Green-Lagrange strain conversion eliminates rigid body motion and assesses deformation relative to the initial state. As shown in Fig. 1B, a coordinate system for quantitative analysis was centered on the optic disc, divided into nasal and temporal hemi-sectors (halves), and further into four concentric zones (R1-R4 having radial extent equal to one disc radius). After strain conversion, we filtered the values by a 25% threshold that clearly excludes artifacts of false detection. In this study, we analyzed strain into three conventional components: horizontal, vertical, and shear[27].

Repeatability.

The entire imaging and analysis protocol was performed twice on 10 subjects selected from the young and older groups to estimate the repeatability of results. Image acquisition in the three gaze positions was repeated in these same subjects after a 30-minute interval. However, rather than registering the central gaze image to the duction images, the first image acquired for each gaze position was registered to the corresponding image in the second set, then processed in the usual manner to interpret any differences as strains quantifying experimental error which would ideally be zero. Conservatively, we chose the maximum absolute value of apparent mean repeatability strain as the applicable error range for each tissue region.

Results

Participants.

A total of 41 subjects participated, comprising 22 younger under age 40 years (mean 26±5 years, ± standard deviation, SD) and 19 older over age 40 years (mean 64±10 years). In the younger group, there were 10 men and 12 women; in the older group, there were 3 men and 16 women. Mean spherical equivalent refractive error of younger subjects was −1.07 ± 1.74 (standard deviation, SD; range) D and that of older subjects was −0.24 ± 2.03 D. Ten subjects of average 33±17 age years participated in repeatability testing.

Repeatability of Strain.

Imaging in central and eccentric gazes was highly repeatable. The repeatability error range for 35° adduction was ±0.10% to ±0.19% for horizontal strain, ±0.06% to ±0.12% for vertical strain, and ±0.02% to ±0.06% for shear strain (Fig. 4). Corresponding values for 35° abduction were ±0.05% to ±0.09% for horizontal, ±0.03% to ±0.06% for vertical, and

±0.01% to ±0.09% for shear strain. Therefore, we considered strain measurements to be valid only when the strain exceeds each corresponding maximum error range derived from this repeatability testing in each relevant hemi-sector. Corresponding ranges from Fig. 4 are illustrated on each subsequent data plot here (Figs. 6 – 8).

Horizontal Strain.

Horizontal and vertical strains are strains caused by horizontal and vertical forces perpendicular to image face, respectively[27]. Tensile strain represents stretching, while compressive strain represents shortening, and each of these can vary according to direction. In younger subjects, tensile horizontal strain in the nasal hemi-disc was significant at 0.70±0.20% during adduction, while strain during abduction was nearly zero (P=0.014, Fig. 5). In the temporal hemi-disc, there was almost no strain during adduction but tensile strain during abduction was 0.28±0.25%. In older subjects, the greatest tensile horizontal strain was in the nasal hemi-disc at 0.82±0.18% in adduction, which was insignificantly higher than the tensile strain in abduction of 0.31±0.13%. Older but not younger subjects exhibited significant compressive strain averaging about 0.72±0.25% during adduction in the temporal hemi-disc, but 0.28±0.25% tensile strain during abduction (P=0.001).

During adduction, horizontal strain occurred only as tension in the nasal peripapillary region that decreased monotonically from the disc to the farthest periphery by an average of 21% and 35% in the younger and older groups, respectively. Tensile strains in the nasal hemi-sector exceeded the repeatability criterion during adduction in all regions analyzed, propagating at least as far as 3 radii from the disc center (Fig. 5).

Vertical Strain.

Vertical strain during horizontal duction was much smaller than horizontal strain (P<0.001, Fig. 6). In younger subjects, vertical strain during adduction consisted of tension in the temporal hemi-disc, but older subjects also included compression in the nasal hemi-disc. During abduction, there was around 1% compressive vertical strain in the disc and multiple regions peripheral to it, more in older than younger subjects (Fig. 6).

Vertical strain in the temporal hemi-disc of older subjects varied significantly with duction direction, being 0.20±0.13% tensile strain during adduction and 0.20±0.11% compressive strain during abduction (P=0.019), but younger subjects did not show this effect. In the nasal hemi-disc, ab- and adduction generated compressive strains of 0.07±0.10% and 0.20±0.12%, respectively. In younger subjects, the temporal hemi-disc showed tensile vertical strain of 0.20±0.12% during adduction, while the nasal hemi-disc showed minimal strains. During abduction in younger subjects, the temporal hemi-disc showed very little strain while the nasal hemi-disc showed 0.05±0.17% compressive strain (Fig. 6).

Shear Strain.

Shear strain is a conventional measure of strain caused by simultaneous, directionally varying forces[2 7]. For example, shear deformation resulting from directionally opposing forces paralleling the tissue surface would change a square shape on the retinal surface into a rhombus. In this study, we followed standard sign convention of shear strain[27]. In both

younger and older groups, some shear strains in the optic disc slightly exceeded vertical strain but were much smaller than horizontal strain (Fig. 7). During adduction, shear strain was similar in the nasal and temporal hemi-discs. In younger subjects, the −0.31±0.17% shear strain in the temporal hemi-disc was greater than −0.07±0.19% shear strain in the nasal hemi-disc. In the older subjects, shear strain in the temporal hemi-disc was less than in the younger subjects at −0.04±0.12%, while shear strain in the nasal hemi-disc was larger at −0.29±0.14%. During abduction by younger subjects, there was −0.29±0.16% shear strain in the temporal hemi-disc and +0.17±0.07% shear strain in the nasal hemi-disc (P=0.019), whereas there was no significant shear strain in older subjects.

Equivalent Strain.

Because compressive and tensile strains that occur locally in may cancel one another in extended regions to suggest little average deformation, we calculated the equivalent Von Mises strain that avoids possible cancellation. Assuming a Poisson ratio close to the incompressible value of 0.5, the equivalent Von Mises strain for the two-dimensional case can be expressed as

$$\varepsilon_{eq} = \frac{2}{3}\sqrt{\varepsilon_{xx}^2 - \varepsilon_{xx}\varepsilon_{yy} + \varepsilon_{yy}^2 + \frac{3}{4}\gamma_{xy}^2} \quad \text{(Eqn. 1)}$$

where ε_{xx} is horizontal strain, ε_{yy} is vertical strain, and γ_{xy} is shear strain. Equivalent strain is plotted in Fig. 8.

Equivalent strain in the optic disc (Region 1) significantly exceeded all other regions for all cases as shown in Fig. 8 (P<0.001). In Region 1, equivalent strain of younger subjects was 2.4±3.2% in adduction, nearly twice as large as the value of 1.3±1.8% in abduction (P<0.001), while older subjects exhibited similar deformations for both adduction (2.2±2.5%) and abduction (2.0±2.4%) cases (P=0.602). Equivalent strains were similar in both hemi-discs (Region 1) for ab- and adduction (Fig. 8, P>0.5).

Shear of Retina and Bruch's membrane Relative to Sclero-choroid.

Occasional subjects have large choroidal vessels that are readily visible through lightly-pigmented overlying retinal pigment epithelia. In one such male subject aged 66 years, it was possible to simultaneously and clearly visualize displacements of both retinal and underlying large choroidal vessels during ab- and adduction. In the nasal but not temporal hemi-retina, large retinal and disc vessels apparently shifted temporally in adduction, while nearby choroidal vessels shifted nasally, by around 40 μm in each case (Fig. 9). There was no differential shift of choroidal vessels in the retina temporal to the disc, nor any differential shift in any region during abduction. This is a clear example of shear perpendicular to the retinal surface that is limited to the nasal peripapillary region. Differential shift of choroidal relative to overlying retinal vessels was suggested in some subjects in whom the choroid was nevertheless obscured by overlying pigment that prevented reliable quantification, but that necessitated masking to limit the primary analysis to retinal vessels only.

Discussion

The current study employed deep learning-based optical flow of confocal SLO images to demonstrate that horizontal eye rotation in healthy adults produces strain in the disc and vessels of the peripapillary retina in which they are largely embedded. This result confirms a previous SLO study that manually measured displacements of vascular bifurcations[14], and extends this approach to quantify strain. Strain measurements are advantageous because they are independent from variations in ocular size and optical magnification and allow more direct biomechanical interpretation. The major finding is that horizontal duction generates significant horizontal and shear strains that are concentrated at the optic disc and diminish with distance from it. Equivalent strains capturing all directions exceed 2% in the optic disc in both younger and older adults. A second novel finding is that vascular displacements in the peripapillary region nasal to the disc appear directionally opposite in the choroid versus those in the overlying retina and optic disc. This phenomenon represents a novel demonstration of mechanical shear between peripapillary retinal and disc tissues, relative to the underlying choroid.

Adduction vs. Abduction.

This study also confirms previous studies[8,13–15,19,28] showing that all strains associated with horizontal duction are concentrated at the optic disc, supporting the inference that the deforming force is imposed by ON structures and gradually declines with distance from the disc (Fig. 5). Consistent with other work[10], greater disc deformation in adduction than abduction (Fig. 5) corresponds to ON tethering in adduction where the ON and its sheath apply counterforce opposing medial rectus muscle contractile force[22,29]. The ON transmits less force to the optic disc when it is in a sinuous configuration during abduction[10,14,19,30].

Effect of Age.

Biological tissues generally stiffen with age[31,32], particularly so for the eye[33–36]. Regionally uniform stiffening is unlikely because tissue constituents vary in composition[37,38]. In nasal retinal hemi-sectors, strain due to horizontal duction in both younger and older adults declined progressively with distance from the disc but more rapidly in older subjects. This suggests that stiffer tissues in older subjects concentrate strain near the disc, while more compliant tissues in younger subjects distribute strain throughout the posterior eye. If this is the case, then peak local tissue stress would be greater in older than younger subjects.

Equivalent strain during adduction Fig. 8 in the temporal hemi-disc was slightly greater in younger than older subjects (Fig. 6). However, older subjects exhibited large compressive horizontal strain on the temporal disc whereas younger subjects show nearly none (Fig. 5). These seemingly contradictory results occur because tensile and compressive strains in younger subjects cancel each other when averaged in regions as large as hemi-discs. On the other hand, the peripapillary retina exhibited low equivalent and horizontal strains in all subjects.

Nasal vs. Temporal Strains in Hemi-regions.

As shown in Fig. 5, horizontal strain during adduction in the nasal hemi-disc rapidly declined with distance from it, whereas strain in the temporal hemi-disc was lower and propagated less peripherally. This again suggests that force due to ON tethering during adduction is transmitted as tensile strain mainly to the nasal hemi-disc and peripapillary retina, but minimally to the temporal hemi-retina. The stability of the temporal hemi-retina is functionally advantageous, since distortion of the high acuity macula would be more likely be visually perceptible than in low acuity nasal retina.

Proposed Resolution of the Direction Paradox.

Previous finite element simulations[8,19,20,22,39] suggest that stress and strain in the sclera caused by adduction occur mainly in the temporal peripapillary region, underlying where peripapillary atrophy frequently occurs[40–43], in contrast to the substantially nasal retinal strains found in this study (Fig. 5). We directly demonstrate here (Fig. 9) that peripapillary retinal vessels on the nasal side of the disc, as well as large disc vessels, move in the opposite direction from underlying choroidal vessels during adduction. This directional difference between retinal and underlying choroidal vessels does not occur on the temporal side of the disc in adduction, nor at all in abduction. We propose that this novel paradox of directional different choroidal and retinal displacement, which constitutes biomechanical shear, may be resolved by considering material property differences among ocular tissues, or by sliding between the laminar coats of the eye, or by both phenomena.

Material properties of the sclera, choroid, and retina differ widely, both from one another and regionally within the same tissues[21,44–46]. An analysis using a consistent methodology showed that the low toe physiological tensile elastic modulus of the sclera was about 100-fold greater than that of the retina, and about 6-fold greater than that of the choroid[44]. Although there are multiple factors that determine the strain distribution, such as structure and force direction, substantially differing stiffnesses among contiguous layers would produce different strain distributions along each layer in response to the same force perturbation as shown in Fig. 10. In particular, since the retina is by far the softest tissue, under mechanical loading it would behave most differently from the underlying, stiffer layers. Moreover, the mechanical boundary conditions for the optic disc and papillary sclera differ from the peripapillary sclera, which is tightly united with high mechanical loading applied to the ON sheath during some eye rotations.

Prior biomechanical studies have typically treated the posterior eye as monolithic, as if the sclera, choroid, retina, and disc were tied together at their interfaces despite potentially differing strains in each tissue[19,39], or only examined the scleral layer[8,20,22]. Bruch's membrane forms a continuous barrier anchored firmly to the ora serrata anteriorly and is continuous except where it is penetrated by its aperture at the optic disc at the Bruch's membrane opening (BMO). While the choroid also is penetrated at the optic disc, the choroid is also mechanically coupled to the underlying sclera via anchors including the four large vortex veins and other neurovascular structures. We thus propose that particularly during adduction, Bruch's membrane, to which the retina is attached via photoreceptor interdigitation with the retinal pigment epithelium, might slide over the choroid to which the

sclera is attached. This sliding would be greatest in the peripapillary region where the sclera is pliable but subject to concentrated force exerted by the ON in large-angle adduction. This concept is consistent with observations that the peripapillary choroid is compressed more by ad- than abduction[47], and that the horizontal diameter of the optic disc is reduced by about 18 μm in adduction[14].

This hypothetical explanation is diagrammed in Fig. 10, illustrating the situation of ON tethering during large adduction that was associated with the greatest disc and peripapillary strains in the current study as well as in finite element simulations[8,20,22]. The superficial layers of Fig. 10 are traced from actual superimposed B-scan OCT of one subject in this study. As the medial rectus (MR) muscle contracts to adduct the globe beyond the 26° angle at which its length redundancy is exhausted, tethering by the ON generates tension at the temporal junction and compression at the nasal junction of the ON sheath with the posterior sclera. However, we proposed the force exerted by the ON on the scleral coat is similarly distributed to the choroid, but differently in Bruch's membrane-retinal complex. This differential distribution arises not only from differences in material properties of these layers but also from differences in their boundary conditions: Bruch's membrane is anchored at the ora serrata anteriorly but may not be completely anchored where ON axons pass through it to exit the eye: the scleral canal and the lamina cribrosa (LC) underlying the optic disc. We propose that the LC and surrounding scleral canal can thus shift differently from BMO during horizontal eye rotations, and that this differential shift can buckle the nasal peripapillary retina and tilt the optic disc. During adduction, multiple investigators have observed that the retina and choroid nasal to the disc buckle anteriorly, while the temporal margin of the disc tilts posteriorly[9,10,30]. Buckling of the nasal sclera forces the nasal hemi-disc and retina anteriorly but compresses the hemi-disc and retina at the temporal edge of the BMO. We here propose that on the nasal side of the disc, peripapillary retinal displacement is consequently different from that of the underlying choroid and sclera because the deeper tissues shift farther nasally than the superficial tissues (as demonstrated in the images in Fig. 10). This shearing would tend in the long term to shift the scleral canal nasally relative to the BMO. Under the impetus of millions of cycles of adduction eye movements over a lifetime, these slight but directionally consistent nasal shifts of the disc and scleral canal might plausibly provide remodeling force to tilt the disc temporally and generate a temporal peripapillary crescent of exposed sclera bereft of overlying Bruch's membrane (gamma zone peripapillary atrophy, PPA) or retinal pigment epithelium (beta zone). Such remodeling of the disc and peripapillary region is widely recognized to occur over the lifespan because the BMO becomes misaligned relative to the scleral canal[48,49], although the relationship to eye movements has not previously been clearly articulated[50]. While the current study deals only with horizontal duction, a combination of adduction with infraduction might direct the forgoing forces obliquely to tilt the disc inferotemporally, and thus drive the configuration described as "disc torsion" that develops in childhood[51] but is particularly common in primary open angle glaucoma[50,52].

Strain Range.

This study demonstrated about 0.8% maximum horizontal strain on optic disc vessels during adduction. This is less than the 4% strain at the lamina cribrosa demonstrated by OCT

during 20° adduction[13], and less the 6% strain at the junction of the ON and peripapillary sclera during 32° adduction predicted by finite element simulation[8]. While peripheral to the presumed source of strain at the optic disc, the delicate retina is nonetheless vulnerable to deformation[44,53–55], and may be damaged by strains exceeding around 2%[44]. The retinal vascular strains measured in the healthy adults studied here were within this physiologic range. However, FEA suggests that adduction tethering can in some cases have greater effects depending on local distributions of ocular tissue stiffness[8].

Strengths and Limitations.

Use of automated image analysis with machine learning is a strength of this study because it minimizes the possibility of investigator bias. A further strength is that strain as an outcome measure is independent of optical magnification and its determinants, such as axial length. Another strength is that this study determined error limits for minimum significant effects by repeatability analysis. The study does, however, have limitations. It should be acknowledged that this exploratory study is limited by its relatively small sample size, and inability to pre-specify sample sizes since there were no prior estimates of effect variances. The current findings are applicable only to healthy adult subjects. Most subjects had choroidal pigmentation that prevented tracking of choroidal vascular displacements. All subjects reported here are adults; we expect to report separately on findings in children.

Summary.

Automated analysis of SLO images of the optic disc and peripapillary region using deep learning-based optic flow demonstrates that horizontal eye rotations in healthy people create significant strains around the optic disc. These strains vary with subject age. Strains are greater in add- than abduction, probably because of tethering of the ON in adduction. In adduction, there is horizontal shear between the nasal peripapillary choroid and the overlying retina.

a. Funding/Support:

National Eye Institute Grants EY008313 and EY00331, and an Unrestricted Grant to the UCLA Department of Ophthalmology from Research to Prevent Blindness. The sponsors or funding organizations had no role in the design or conduct of this research.

b. Financial Disclosures:

Joseph Park, Seongjin Lim, and Joseph L. Demer: National Eye Institute Grants EY008313 and EY00331, and an Unrestricted Grant to the UCLA Department of Ophthalmology from Research to Prevent Blindness.

Financial Support

This project was supported by U.S. National Eye Institute Grants EY008313 and EY000331, Research Year Grant 20180194 from Inje University, and an unrestricted grant from Research to Prevent Blindness. The funding organizations had no role in the design or conduct of this research.

References

1. Epelboim J, Steinman RM, Kowler E, Pizlo Z, Erkelens CJ, Collewijn H. Gaze-shift dynamics in two kinds of sequential looking tasks. Vision Res. Sep 1997;37(18):2597–2607. [PubMed: 9373691]

2. Wu CC, Kowler E. Timing of saccadic eye movements during visual search for multiple targets. J Vis. Sep 18 2013;13(11)
3. Robinson DA. Control of eye movements. vol 2. Williams & Wilkins; 1981:1275–1320.
4. Leclair-Visonneau L, Oudiette D, Gaymard B, Leu-Semenescu S, Arnulf I. Do the eyes scan dream images during rapid eye movement sleep? Evidence from the rapid eye movement sleep behaviour disorder model. Brain. Jun 2010;133(Pt 6):1737–1746. [PubMed: 20478849]
5. Anastasopoulos D, Ziavra N, Hollands M, Bronstein A. Gaze displacement and inter-segmental coordination during large whole body voluntary rotations. Exp Brain Res. Mar 2009;193(3):323–336. [PubMed: 19002676]
6. von Helmholtz H Helmholtz's treatise on physiological optics. translated from the Third German Edition ed. vol 1. The Optical Society of America; 1924:1698.
7. Friedman B Mechanics of optic nerve traction on the retina during ocular rotation. Arch Ophthalmol. 1941;25(4):564–575.
8. Park J, Shin A, Demer JL. Finite element modeling of effects of tissue property variation on human optic nerve tethering during adduction. Sci Rep. Nov 8 2022;12(1):18985. [PubMed: 36347907]
9. Sibony PA. Gaze evoked deformations of the peripapillary retina in papilledema and ischemic optic neuropathy. Invest Ophthalmol Vis Sci. Sep 1 2016;57(11):4979–4987. [PubMed: 27661851]
10. Suh SY, Le A, Shin A, Park J, Demer JL. Progressive deformation of the optic nerve head and peripapillary structures by graded horizontal duction. Invest Ophthalmol Vis Sci. Oct 1 2017;58(12):5015–5021. [PubMed: 28973373]
11. Suh SY, Clark RA, Demer JL. Optic nerve sheath tethering in adduction occurs in esotropia and hypertropia, but not in exotropia. Invest Ophthalmol Vis Sci. Jun 1 2018;59(7):2899–2904. [PubMed: 30025141]
12. Sibony PA, Wei J, Sigal IA. Gaze-evoked deformations in optic nerve head drusen: Repetitive shearing as a potential factor in the visual and vascular complications. Ophthalmology. Jun 2018;125(6):929–937. [PubMed: 29361354]
13. Wang X, Beotra MR, Tun TA, et al. In vivo 3-dimensional strain mapping confirms large optic nerve head deformations following horizontal eye movements. Invest Ophthalmol Vis Sci. Oct 1 2016;57(13):5825–5833. [PubMed: 27802488]
14. Le A, Chen J, Lesgart M, Gawargious BA, Suh SY, Demer JL. Age-dependent deformation of the optic nerve head and peripapillary retina by horizontal duction. Am J Ophthalmol. Jan 2020;209:107–116. [PubMed: 31472159]
15. Demer JL. Optic nerve sheath as a novel mechanical load on the globe in ocular duction. Invest Ophthalmol Vis Sci. Apr 2016;57(4):1826–1838. [PubMed: 27082297]
16. Clark RA, Suh SY, Caprioli J, et al. Adduction-induced strain on the optic nerve in primary open angle glaucoma at normal intraocular pressure. Curr Eye Res. Apr 2021;46(4):568–578. [PubMed: 32911989]
17. Demer JL, Clark RA, Suh SY, et al. Optic nerve traction during adduction in open angle glaucoma with normal versus elevated intraocular pressure. Curr Eye Res. Feb 2020;45(2):199–210. [PubMed: 31453714]
18. Shang K, Dai Y, Liu H, Qu X, Wen W, Jonas JB. Optic disc shape in patients with long-lasting unilateral esotropia and exotropia. BMC Ophthalmol. Aug 16 2019;19(1):185. [PubMed: 31420011]
19. Wang X, Rumpel H, Lim WE, et al. Finite element analysis predicts large optic nerve head strains during horizontal eye movements. Invest Ophthalmol Vis Sci. May 1 2016;57(6):2452–2462. [PubMed: 27149695]
20. Shin A, Yoo L, Park J, Demer JL. Finite element biomechanics of optic nerve sheath traction in adduction. J Biomech Eng. Oct 1 2017;139(10):1010101–10101010. [PubMed: 28787473]
21. Park J, Shin A, Jafari S, Demer JL. Material properties and effect of preconditioning of human sclera, optic nerve, and optic nerve sheath. Biomech Model Mechanobiol. Aug 2021;20(4):1353–1363. [PubMed: 33877503]
22. Jafari S, Lu Y, Park J, Demer JL. Finite element model of ocular adduction by active extraocular muscle contraction. Invest Ophthalmol Vis Sci. Jan 4 2021;62(1):1.

23. Bay H, Ess A, Tuytelaars T, Van Gool L. Speeded-up robust features (surf). Comput Vis Image Und. Jun 2008;110(3):346–359.
24. Teed Z, Deng J. RAFT: Recurrent all-pairs field transforms for optical flow. presented at: European Conference on Computer Vision; 11.03.2020 2020; Glasgow, UK.
25. Azad R, Asadi-Aghbolaghi M, Fathy M, Escalera S. Attention deeplabv3+: Multi-level context attention mechanism for skin lesion segmentation. Springer International Publishing; 2020:251–266.
26. Song YL S; Kim YT; Park YM; Jo DA; Bae NH; Lee SJ; Choi BG; Im SG; Kim HU; Lee KG;. Deep learning enables accurate analysis of images generated from droplet-based digital polymerase chain reaction (dpcr). Sens Actuators B Chem. 2023;379:133241.
27. Beer FP, Johnston ER, DeWolf JT, Mazurek DF. Mechanics of materials. 7 ed. McGraw-Hill Education; 2011.
28. Demer JL, Clark RA, Suh SY, et al. Magnetic resonance imaging of optic nerve traction during adduction in primary open-angle glaucoma with normal intraocular pressure. Invest Ophthalmol Vis Sci. Aug 1 2017;58(10):4114–4125. [PubMed: 28829843]
29. Demer JL. Inflection in inactive lateral rectus muscle: Evidence suggesting focal mechanical effects of connective tissues. Invest Ophthalmol Vis Sci. Nov 2008;49(11):4858–4864. [PubMed: 18599563]
30. Chang MY, Shin A, Park J, et al. Deformation of optic nerve head and peripapillary tissues by horizontal duction. Am J Ophthalmol. Feb 2017;174:85–94. [PubMed: 27751810]
31. Miller RT. Mechanical properties of basement membrane in health and disease. Matrix Biol. Jan 2017;57–58:366–373.
32. Sherratt MJ. Age-related tissue stiffening: Cause and effect. Adv Wound Care (New Rochelle). Feb 2013;2(1):11–17. [PubMed: 24527318]
33. Geraghty B, Jones SW, Rama P, Akhtar R, Elsheikh A. Age-related variations in the biomechanical properties of human sclera. J Mech Behav Biomed Mater. Dec 2012;16:181–191. [PubMed: 23182387]
34. Coudrillier B, Tian J, Alexander S, Myers KM, Quigley HA, Nguyen TD. Biomechanics of the human posterior sclera: Age- and glaucoma-related changes measured using inflation testing. Invest Ophthalmol Vis Sci. Apr 2 2012;53(4):1714–1728. [PubMed: 22395883]
35. Booij JC, Baas DC, Beisekeeva J, Gorgels TG, Bergen AA. The dynamic nature of bruch's membrane. Prog Retin Eye Res. Jan 2010;29(1):1–18. [PubMed: 19747980]
36. Albon J, Karwatowski WS, Easty DL, Sims TJ, Duance VC. Age related changes in the non-collagenous components of the extracellular matrix of the human lamina cribrosa. Br J Ophthalmol. Mar 2000;84(3):311–317. [PubMed: 10684844]
37. Muiznieks LD, Keeley FW. Molecular assembly and mechanical properties of the extracellular matrix: A fibrous protein perspective. Biochim Biophys Acta. Jul 2013;1832(7):866–875. [PubMed: 23220448]
38. Yue B Biology of the extracellular matrix: An overview. J Glaucoma. Oct-Nov 2014;23(8 Suppl 1):S20–23. [PubMed: 25275899]
39. Wang X, Fisher LK, Milea D, Jonas JB, Girard MJ. Predictions of optic nerve traction forces and peripapillary tissue stresses following horizontal eye movements. Invest Ophthalmol Vis Sci. Apr 1 2017;58(4):2044–2053. [PubMed: 28384725]
40. Jonas JB, Fernandez MC, Naumann GO. Glaucomatous parapapillary atrophy. Occurrence and correlations. Arch Ophthalmol. Feb 1992;110(2):214–222. [PubMed: 1736871]
41. Sugiyama K, Tomita G, Kitazawa Y, Onda E, Shinohara H, Park KH. The associations of optic disc hemorrhage with retinal nerve fiber layer defect and peripapillary atrophy in normal-tension glaucoma. Ophthalmology. Nov 1997;104(11):1926–1933. [PubMed: 9373128]
42. Uchida H, Ugurlu S, Caprioli J. Increasing peripapillary atrophy is associated with progressive glaucoma. Ophthalmology. Aug 1998;105(8):1541–1545. [PubMed: 9709771]
43. Manjunath V, Shah H, Fujimoto JG, Duker JS. Analysis of peripapillary atrophy using spectral domain optical coherence tomography. Ophthalmology. Mar 2011;118(3):531–536. [PubMed: 20920826]

44. Chen K, Rowley AP, Weiland JD, Humayun MS. Elastic properties of human posterior eye. J Biomed Mater Res A. Jun 2014;102(6):2001–2007. [PubMed: 23852923]
45. Ferrara M, Lugano G, Sandinha MT, Kearns VR, Geraghty B, Steel DHW. Biomechanical properties of retina and choroid: A comprehensive review of techniques and translational relevance. Eye (Lond). Jul 2021;35(7):1818–1832. [PubMed: 33649576]
46. Rohrbach D, Ito K, Lloyd HO, et al. Material properties of human ocular tissue at 7-microm resolution. Ultrason Imaging. Sep 2017;39(5):313–325. [PubMed: 28675987]
47. Chen JY, Le A, De Andrade LM, Goseki T, Demer JL. Compression of the choroid by horizontal duction. Invest Ophthalmol Vis Sci. Oct 1 2019;60(13):4285–4291. [PubMed: 31618765]
48. Kim M, Choung HK, Lee KM, Oh S, Kim SH. Longitudinal changes of optic nerve head and peripapillary structure during childhood myopia progression on oct: Boramae myopia cohort study report 1. Ophthalmology. Aug 2018;125(8):1215–1223. [PubMed: 29550000]
49. Lee KM, Choung HK, Kim M, Oh S, Kim SH. Positional change of optic nerve head vasculature during axial elongation as evidence of lamina cribrosa shifting: Boramae myopia cohort study report 2. Ophthalmology. Aug 2018;125(8):1224–1233. [PubMed: 29544962]
50. Chan PP, Zhang Y, Pang CP. Myopic tilted disc: Mechanism, clinical significance, and public health implication. Review. Frontiers in Medicine. 2023-February-09 2023;10
51. Kim JA, Kim TW, Lee EJ, Hwang JM. Development of optic disc torsion in children. Korean J Ophthalmol. Apr 2019;33(2):173–180. [PubMed: 30977327]
52. Ha A, Chung W, Shim SR, et al. Association of optic disc tilt and torsion with open-angle glaucoma progression risk: Meta-analysis and meta-regression analysis. Am J Ophthalmol. Dec 2021;232:30–39. [PubMed: 34107309]
53. Wollensak G, Spoerl E, Grosse G, Wirbelauer C. Biomechanical significance of the human internal limiting lamina. Retina. Oct 2006;26(8):965–968. [PubMed: 17031303]
54. Chen K, Rowley AP, Weiland JD. Elastic properties of porcine ocular posterior soft tissues. J Biomed Mater Res A. May 2010;93(2):634–645. [PubMed: 19591238]
55. Shahbazi S, Mokhtari-Dizaji M, Mansori MR. Noninvasive estimation of the ocular elastic modulus for age-related macular degeneration in the human eye using sequential ultrasound imaging. Ultrasonics. Feb 2012;52(2):208–214. [PubMed: 21944993]

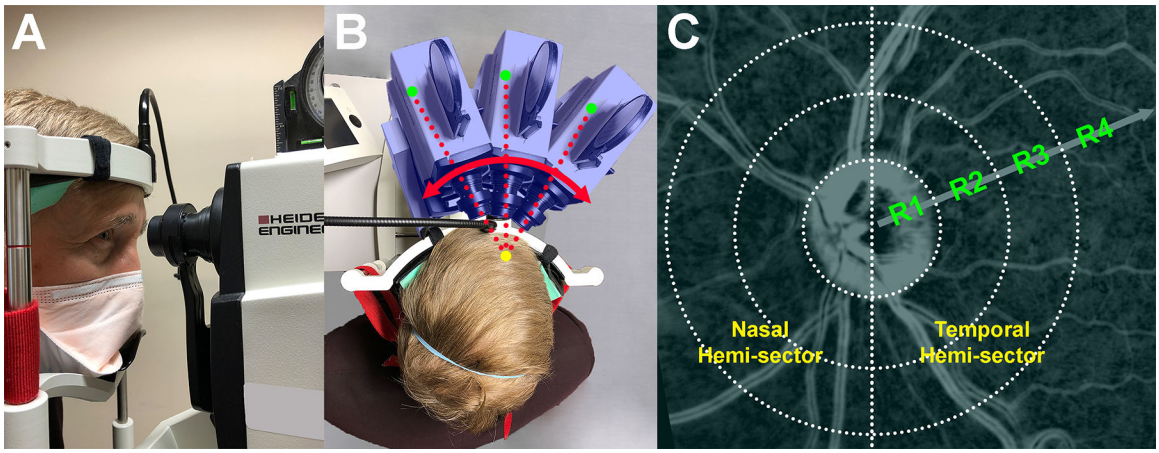

Fig. 1.

Experimental setup. (A) Side view. A red strap and wedge shape foams help to secure the firm fixation of the subject's head while the experiment is performed. (B) Top view. Azimuth rotation camera head enables scanning in central gaze, and in 35° ab- and adduction. Yellow, red, and green dots indicate the location of the subject's right eye, gaze directions, and internal target, respectively. The nasally biased offset of the camera's internal target was considered to find a proper angle of rotation. (C) Four regions (R1-R4) were annuli defined by disc radius from the disc center. R1 represents the disc. Each region was divided into nasal and temporal hemi-sectors.

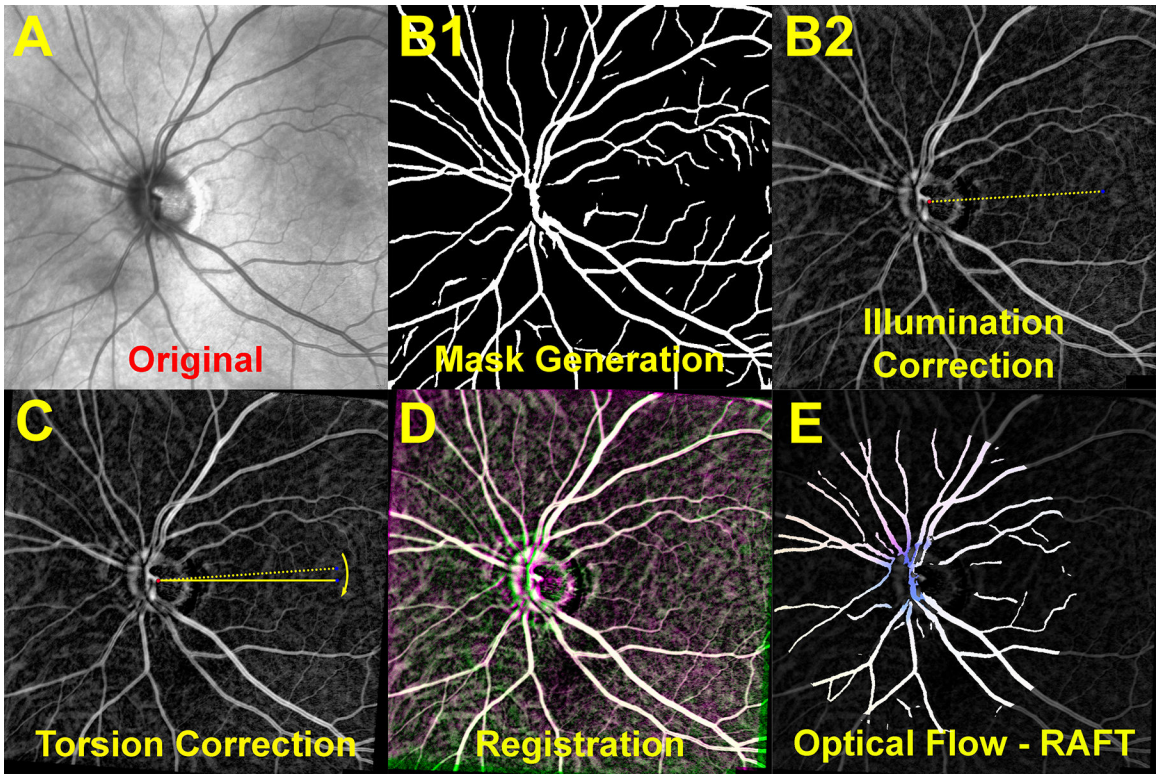

Fig. 2.

Image processing example. (A) Raw images of central gaze, abduction and adduction were obtained. (B1) A retinal vessel mask was generated using a convolutional neural network, and set aside for the final analytic step. (B2) Nonuniform illumination in the original image was corrected by subtracting the local background level. (C) The image was rotated to set the disk foveal angle to the horizontal. (D) Images obtained in ab- and adduction were registered to the central gaze image. (E) Sets of registered images were processed by the RAFT deep learning-based optical flow algorithm to estimate the displacement field. Then, the mask generated in B1 was used to select only displacement of retinal vessels.

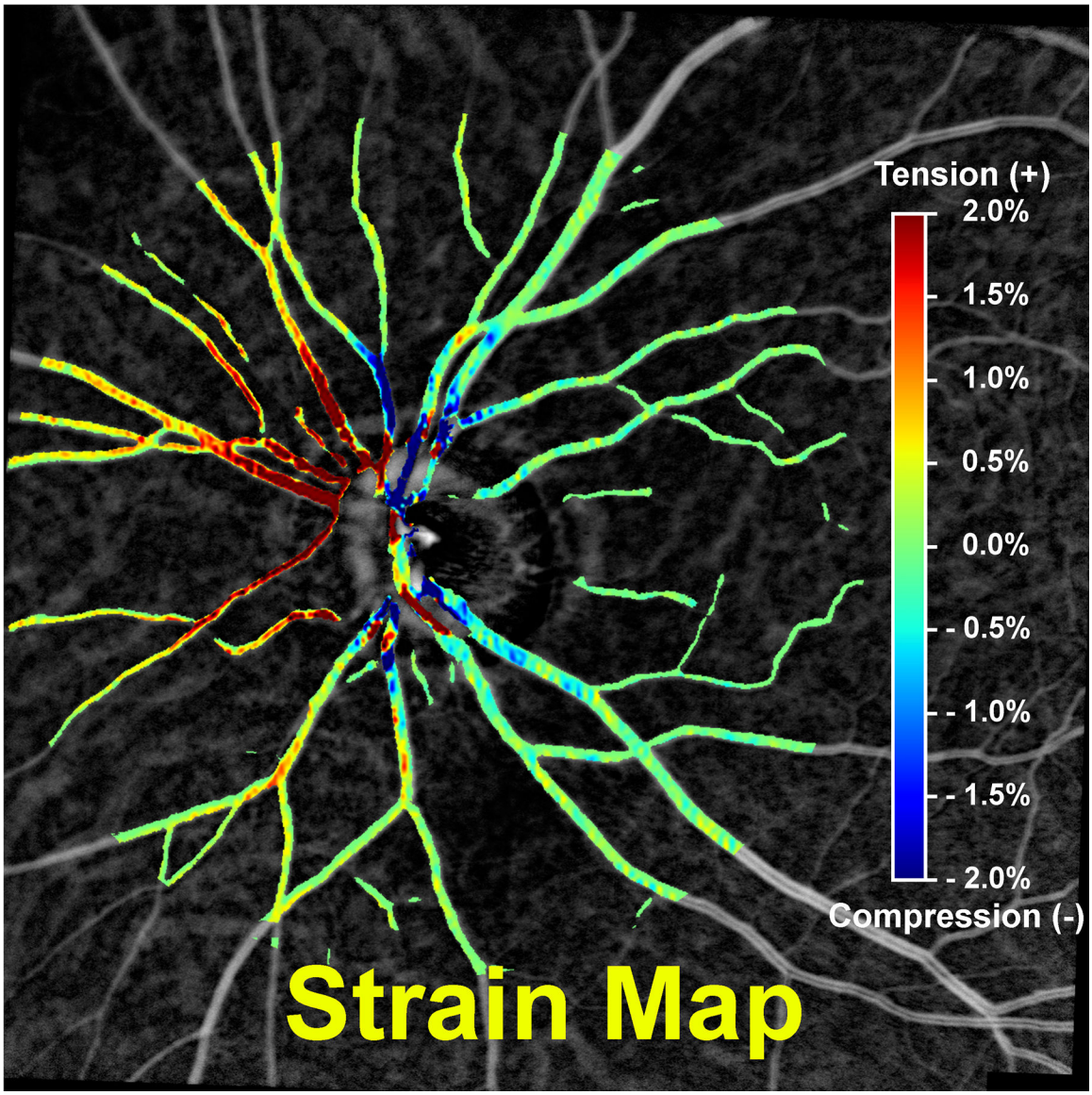

Fig. 3.

Representative strain map of a 67-year-old adult induced by 35° adduction. Positive and negative numbers on the heat map tensile and compressive strain, respectively.

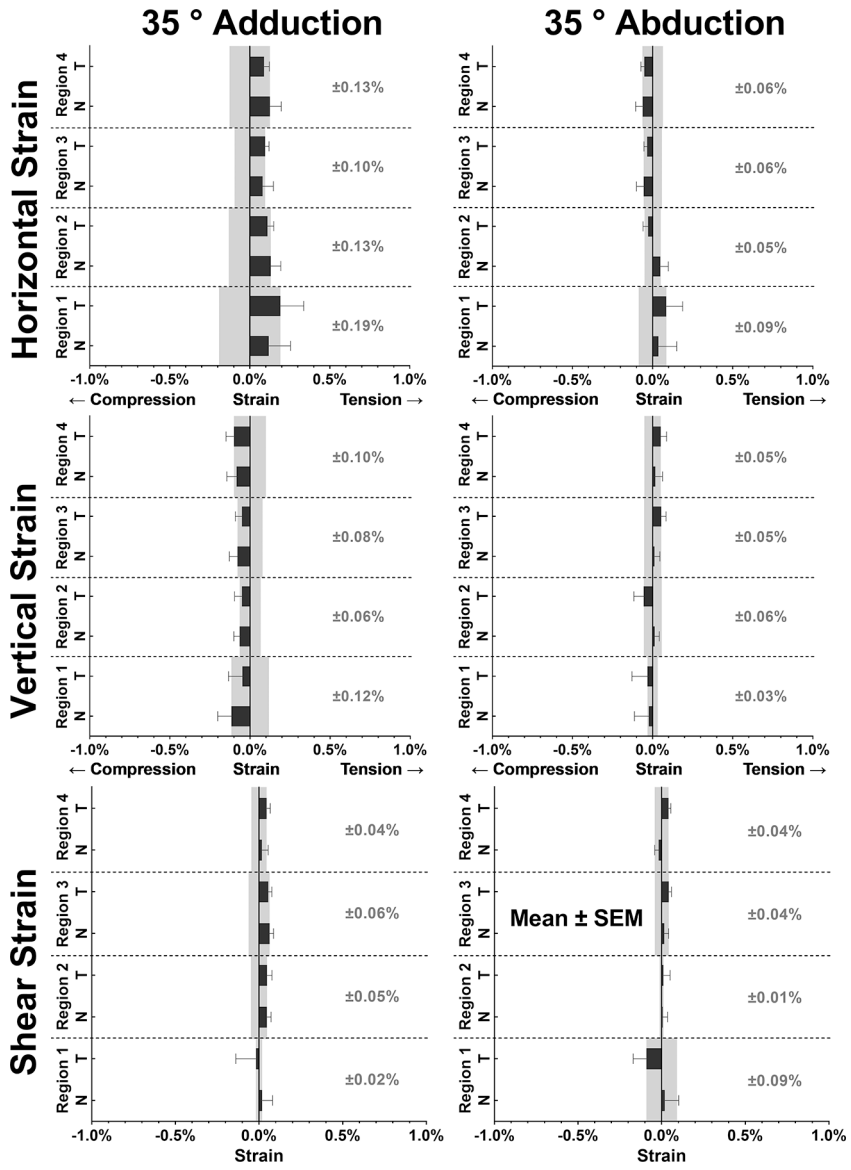

Fig. 4.

Repeatability of strain measurement in 35° adduction and abduction. Differences in duplicate image acquisitions for the same gaze directions are plotted as apparent strain in horizontal, vertical, and shear directions. The gray shaded area and numbers represent the range of the error in nasal (N) and temporal (T) hemi-sectors. In the absence of experimental errors, all values would ideally be zero.

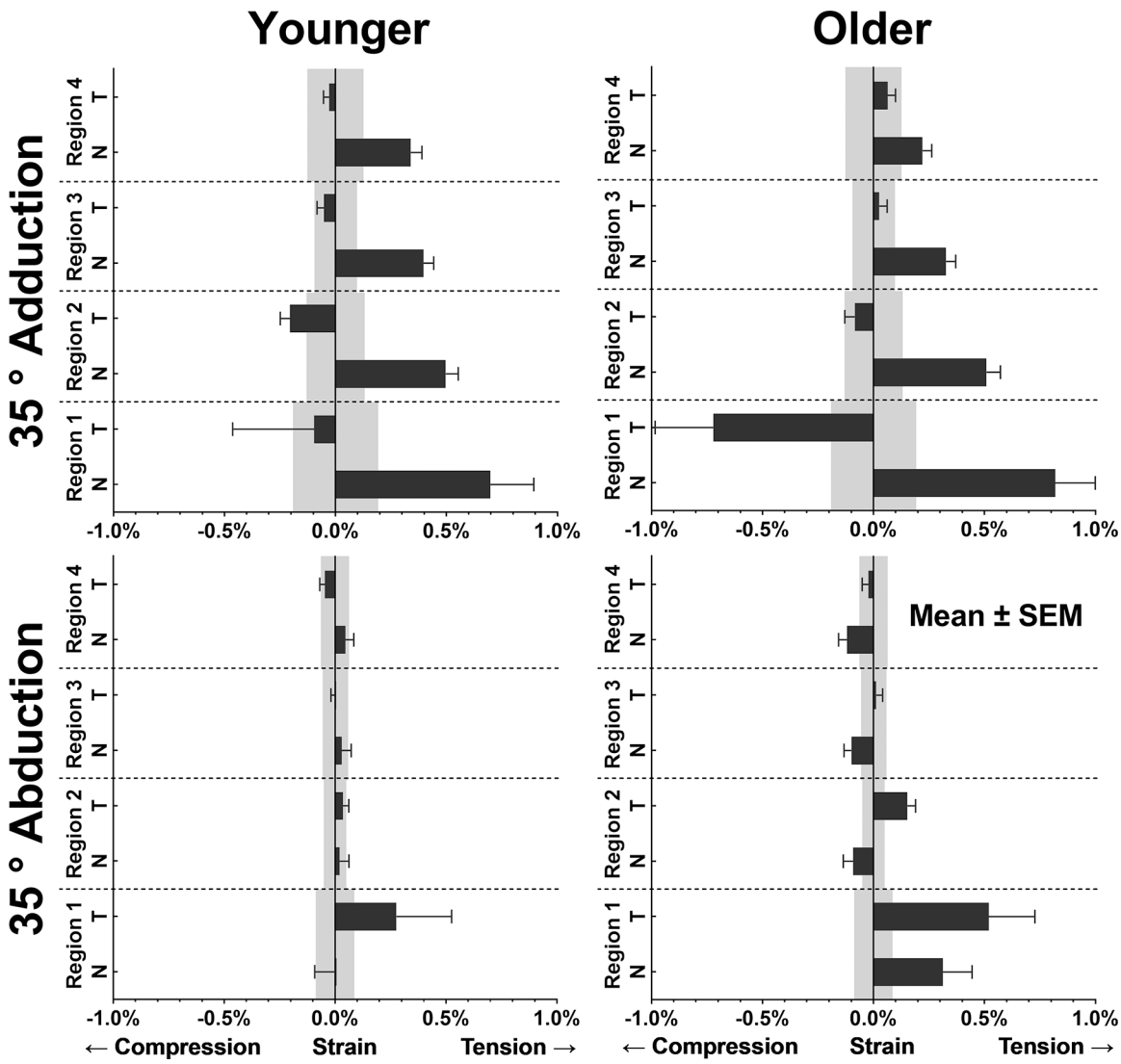

Fig. 5.

Horizontal strains due to 35° add- and abduction. Gray shaded areas represent error ranges from repeatability testing. SEM – standard error of the mean. N – nasal hemi-sector. T – temporal hemi-sector.

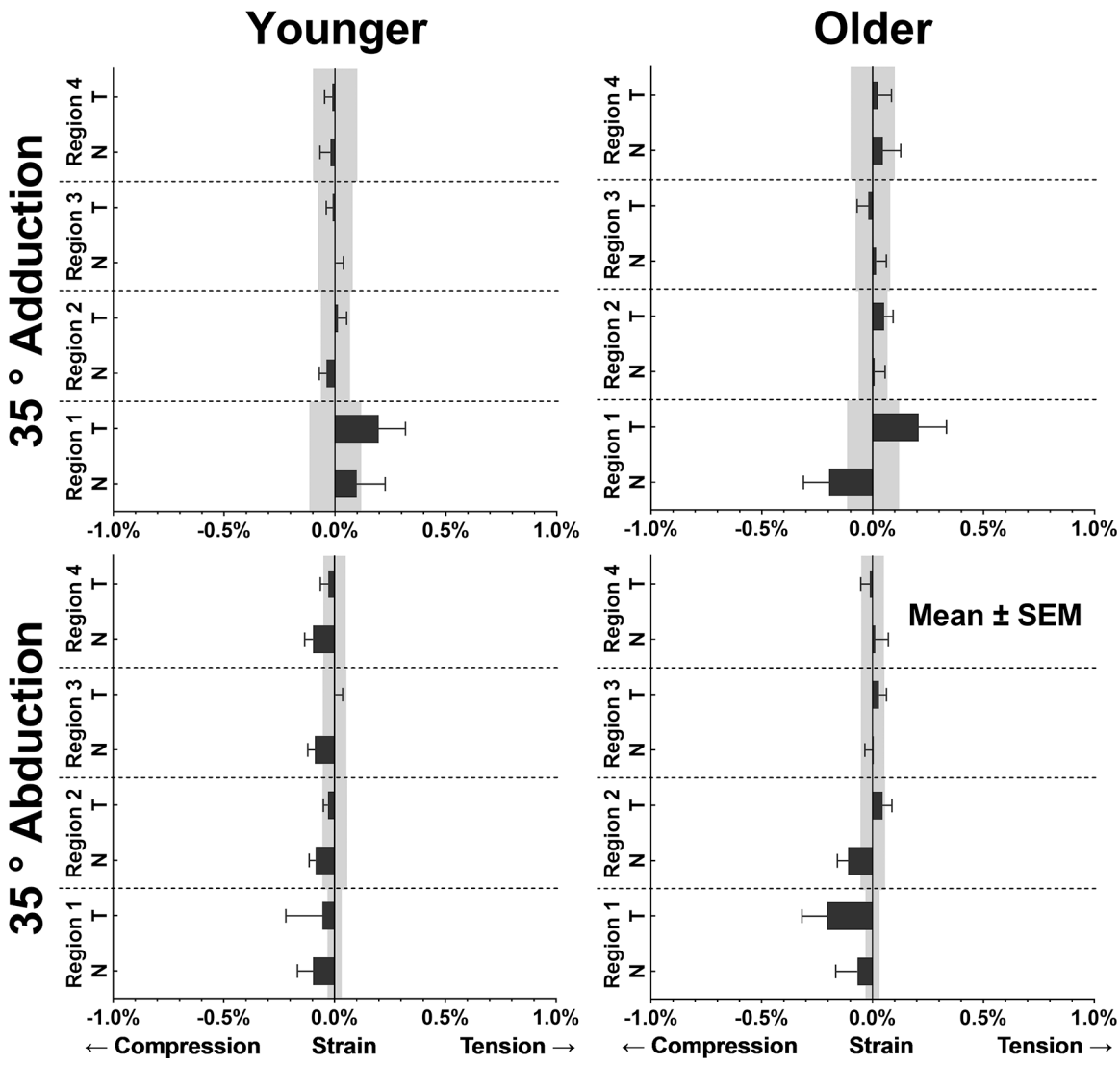

Fig. 6.

Vertical strains due to 35° add- and abduction Gray shaded areas represent error ranges from repeatability testing.

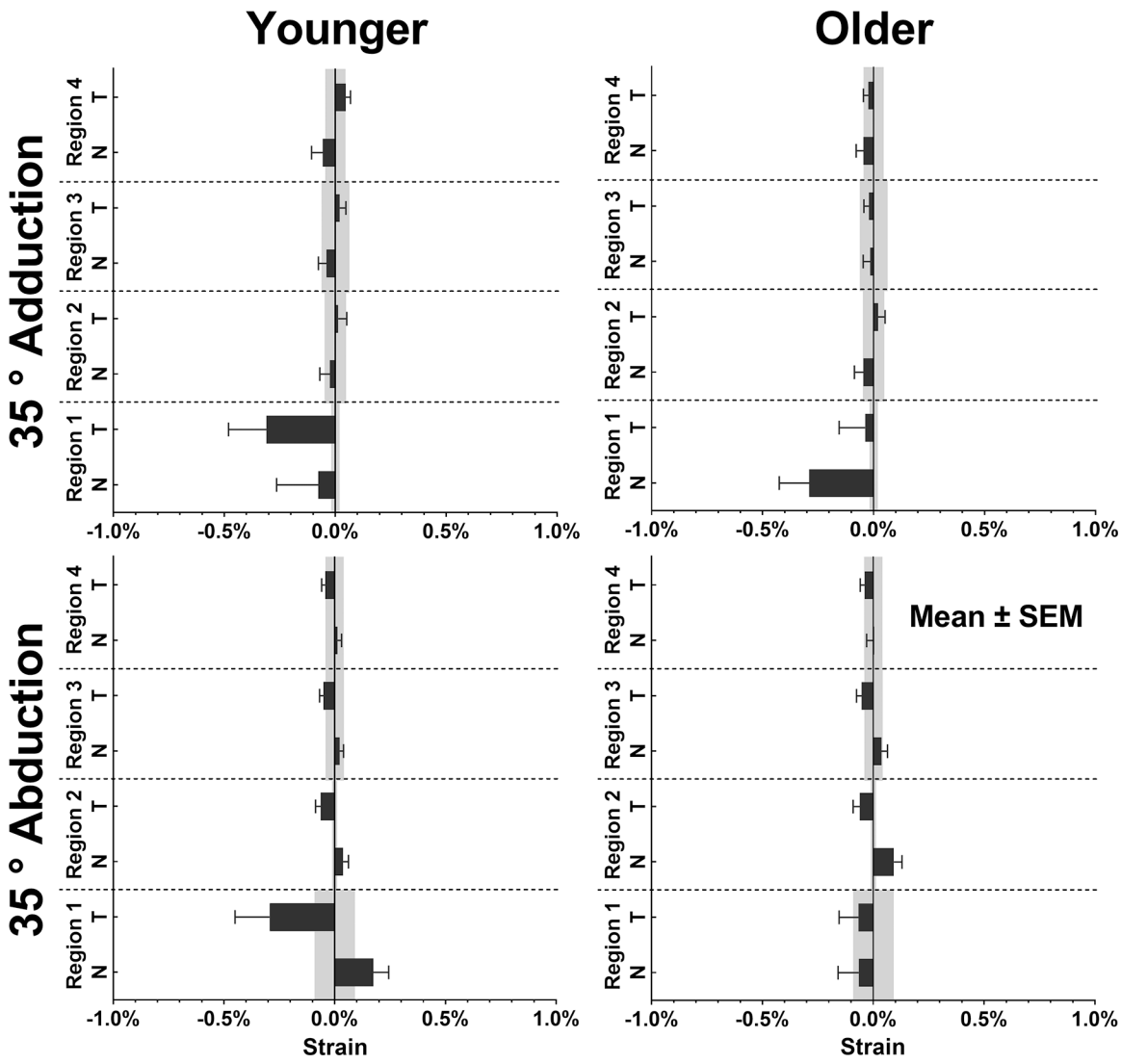

Fig. 7.

Shear strains of young and older adults in 35° add- and abduction. Gray shaded areas represent the error ranges from repeatability testing.

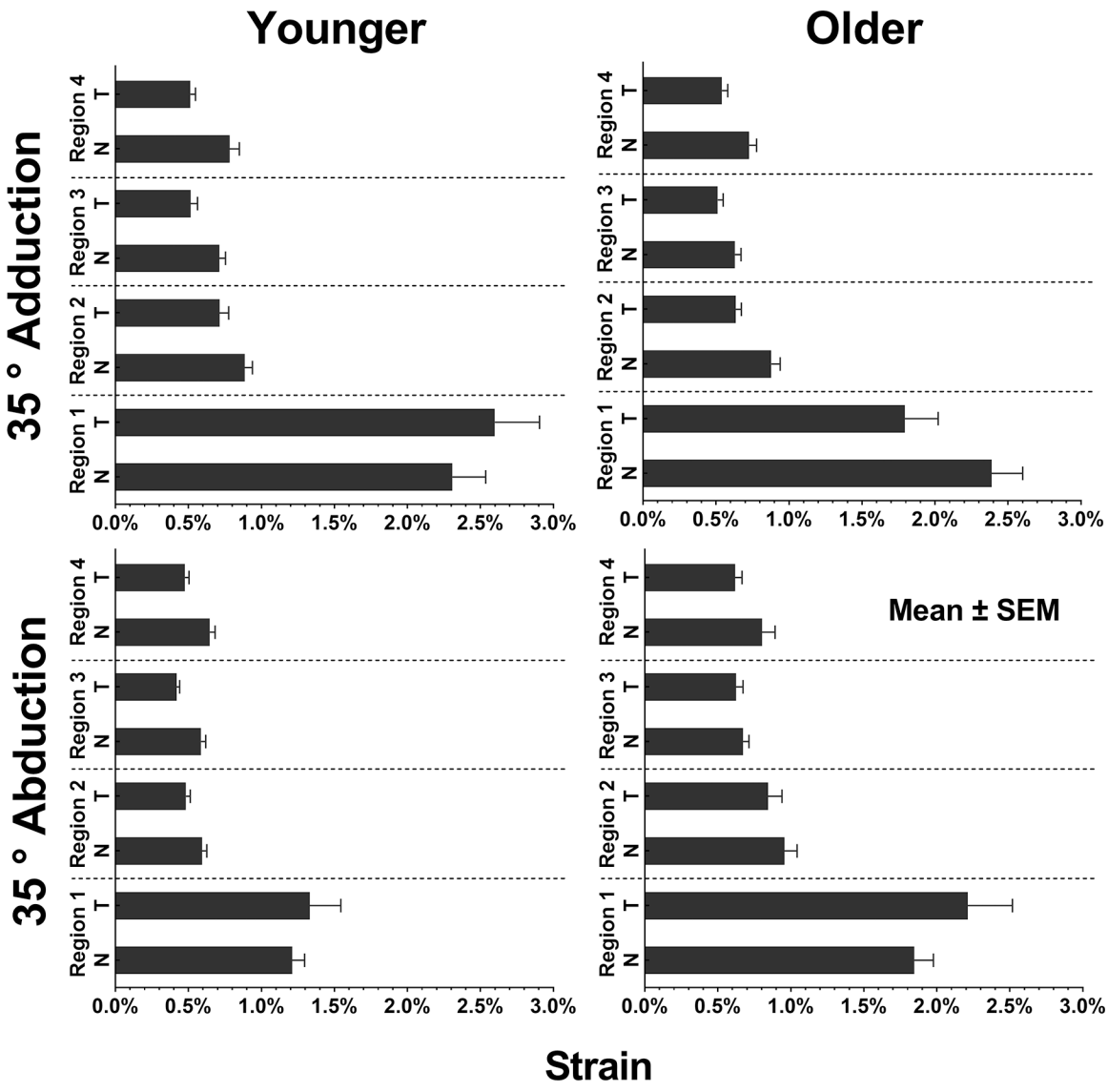

Fig. 8.
Equivalent Von Mises strains of younger and older adults.

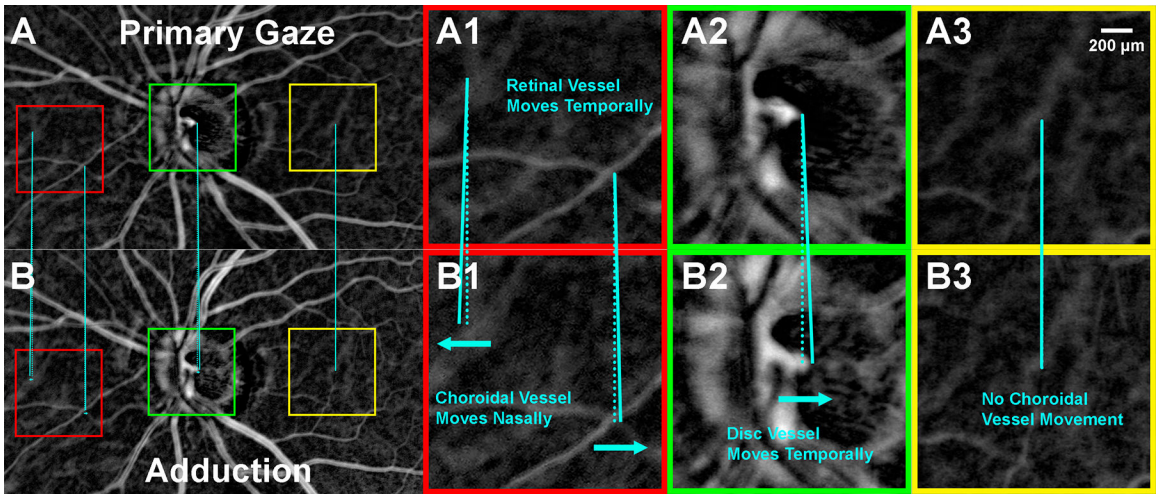

Fig. 9.

Opposite movement of retinal and choroidal vessel during adduction. Scanning laser ophthalmoscope (SLO) images (A) in primary gaze and (B) in adduction; Magnification of temporal hemi-sector (A1) in primary gaze and (B1) in adduction; Disc magnification (A2) in primary gaze and (B2) in adduction; Temporal hemi-sector magnification (A3) in primary gaze and (B3) in adduction. In adduction, retinal vessel on the nasal hemi-sector moves temporally while nasal choroidal & disc vessel moves temporally. There was no movement of the choroidal vessel on the temporal hemi-sector.

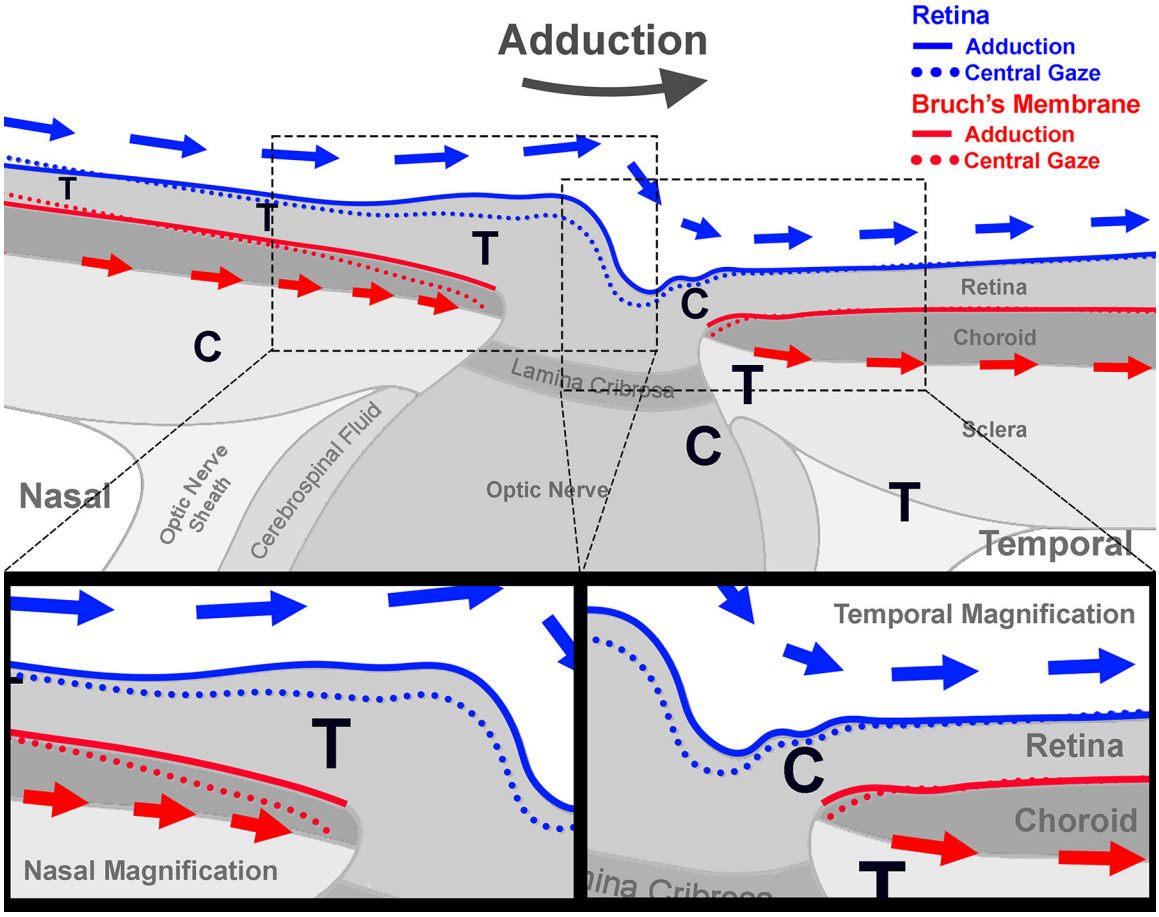

Fig. 10.

Proposed mechanism deformations produced by optic nerve tethering during adduction. Blue dotted and solid lines indicate the retinal surface in central gaze and adduction, respectively, and red dotted and solid lines indicate Bruch's membrane in central gaze and adduction, respectively. The T represents tensile strain and the C represents compressive strain. Letter size indicates relative strain magnitude. Length of the blue arrow indicates the amount of relative motion of the retina, and the red arrow indicates that of the choroid and sclera. Note that the nasal retina and nasal aspect of the optic nerve head move more than the nasal peripapillary choroid, while the two layers move similarly on the temporal aspect of the nerve head.